Journal of Hydrology 403 (2011) 352–359

Contents lists available at ScienceDirect

Journal of Hydrology

journal homepage: www.elsevier.com/locate/jhydrol

Non-isothermal, three-phase simulations of near-surface flows in a model permafrost system under seasonal variability and climate change

Andrew Frampton [a,b,*], Scott Painter [c], Steve W. Lyon [a,b], Georgia Destouni [a,b]

[a] Department of Quaternary Geology & Physical Geography, Stockholm University, Sweden
[b] Bert Bolin Centre for Climate Research, Stockholm University, Sweden
[c] Computational Earth Sciences Group, Earth and Environmental Sciences Division, Los Alamos National Laboratory, USA

ARTICLE INFO

Article history:
Received 24 September 2010
Received in revised form 7 February 2011
Accepted 3 April 2011
Available online 13 April 2011
This manuscript was handled by P. Baveye, Editor-in-Chief

Keywords:
Permafrost hydrology
Three-phase flow
Seasonal variability
Climate change
Runoff

SUMMARY

Permafrost responses to a changing climate can affect hydrological and biogeochemical cycling, ecosystems and climate feedbacks. We have simulated a model permafrost system in the temperature range associated with discontinuous permafrost focusing on interactions between permafrost and hydrology using a non-isothermal, three-phase model of water migration coupled to heat transport in partially frozen porous media. We explore the subsurface hydraulic property controls on the formation and dynamics of permafrost, and how this impacts seasonal variability of subsurface runoff to surface waters. For all subsurface conditions considered, the main common hydrological signal of permafrost degradation in a warming trend is decreasing seasonal variability of water flow. This is due to deeper and longer flow pathways with increasing lag times from infiltration or thawing through subsurface flow to surface water discharge. These results show how physically based numerical modelling can be used to quantitatively and qualitatively improve the understanding of how permafrost thawing relates to, and may be detected in, hydrological data. This is advantageous since hydrological data is considerably easier to obtain, may be available in longer time series, and generally reflects larger-scale conditions than direct permafrost observations.

© 2011 Elsevier B.V. All rights reserved.

1. Introduction

Stream flows in cold regions are integral products of water flow through different water subsystems (soil water, groundwater, stream networks) and cryosphere components (glaciers, permafrost), of which all may change in a changing climate. Permafrost clearly changes in a changing climate (Nelson, 2003; Hinzman et al., 2005; Zhang et al., 2005; Anisimov and Reneva, 2006), with effects on hydrological and biogeochemical cycling, ecosystems, and climate feedbacks (MacLean et al., 1999; Nelson, 2003; Hinzman et al., 2005; Smedberg et al., 2006; McNamara et al., 2008; Woo et al., 2008; Cui and Graf, 2009; Francis et al., 2009; Frey and McClelland, 2009). The hydrological flow responses to permafrost change constitute essential links in all these effects. However, these links are largely unresolved because it is difficult to relate observed stream flow changes directly and specifically to permafrost change, due to the flow system complexity (Nelson, 2003; Hinzman et al., 2005; Francis et al., 2009), and the difficulty and inadequacy of field observation of both permafrost and hydrology in permafrost regions (Woo et al., 2008; Bring and Destouni, 2009; Arctic-HYDRA, 2010).

Some progress has been made in relating changes in hydrological storage and discharge characteristics to seasonal active layer variability (Carey and Woo, 2001; Yamazaki et al., 2006) and long-term permafrost thawing (Lyon et al., 2009; Lyon and Destouni, 2010). However, much uncertainty remains, for example regarding the development of arctic river discharges and main causes for their change (Peterson et al., 2002; Manabe et al., 2004; Wu et al., 2005; McClelland et al., 2006; Dyurgerov et al., 2010). An overview of recent advancements in permafrost modelling is provided by Riseborough et al. (2008), which highlights the need of adapting transient numerical models. Also, Woo et al. (2008) emphasize the need to improve the modelling of subsurface hydrology interactions with active layer dynamics. There is therefore a need for studies of water flows and their potential changes in permafrost regions that are based on a fundamental physical understanding of subsurface hydrology as well as ice formation and thawing processes.

Even though the current generation of numerical permafrost models are able to handle greater complexity than analytic or semi-analytic approaches, these have generally been constrained to one-dimensional domains of vertical extent only (Riseborough

* Corresponding author at: Department of Quaternary Geology & Physical Geography, Stockholm University, Sweden.
E-mail address: andrew.frampton@natgeo.su.se (A. Frampton).

0022-1694/$ - see front matter © 2011 Elsevier B.V. All rights reserved.
doi:10.1016/j.jhydrol.2011.04.010

et al., 2008). This imposes obvious limitations to simulated results, as three-dimensional hydro-thermal (and mechanical) effects are neglected; hence, there is a need to improve the realism of numerical models. A notable exception is found in the recent study by Bense et al. (2009), where a two-dimensional finite element numerical model is used to simulate long-term permafrost degradation in a warming climate. They were able to link increase in base flow to the presence of thin, shallow groundwater systems residing above a permafrost layer, and also predicted re-activation of dormant groundwater below the layer for a warming climate. In their analysis a fully saturated aquifer was assumed, i.e. the water table was assumed to coincide with the top surface boundary, which neglects effects of air–water phase dynamics occurring in unsaturated regions. Also, no seasonal variability in surface temperature was implemented, and further only homogenous porous media scenarios were analyzed, considering three cases of aquifer permeability values.

In our study, we have conducted a series of physically based, two-dimensional simulations of permafrost and hydrological change under both seasonal variability as well as a warming trend in surface temperature. We have used the recently developed MarsFlo code (Painter, 2011), which is a non-isothermal, three-phase model of water migration coupled to heat transport in partially frozen porous media, and analyzed flow discharge in various homogeneous and heterogeneous soil textures representing subsurface conditions typically occurring in arctic and sub-arctic regions. The main aim of the simulations was to investigate the capabilities of physically based numerical modelling to enhance the understanding of the interactions between permafrost thawing and near-surface water flows in continuous and discontinuous permafrost environments. With this aim, the simulations focused on quantifying permafrost and associated soil and ground water flow responses, subject to seasonal variability and long-term increase of surface temperature in different homogeneous and heterogeneous soil and groundwater systems.

2. Method

2.1. General modelling theory

The MarsFlo code (Painter, 2011), originally applied to simulation of Martian hydrology (Painter and Grimm, 2007; Grimm and Painter, 2009), has in this study been adapted to simulate permafrost and hydrology interactions on Earth by appropriate assignment of physical and constitutive parameters. The code solves non-isothermal (heat transport) conservation equations for two member components; water, which can occur in the ice, liquid and vapour phases, and a gas species, which can occur in the gas phase and be dissolved in water. For the adaptation considered in this study, the gas species is used to represent air and is assigned the properties of nitrogen. In the following a brief presentation of the governing equations of the MarsFlo model is given; for a complete description see Painter (2011), describing also the MarsFlo code evaluation and validation against other relevant numerical codes and analytical solutions where applicable.

Using the extended Darcy's law for multiphase flow, the mass conservation equations for the two member components $\beta = w, a$ (representing water and the air species) in the given phase $p = l, g, i$ (representing liquid, gas, and ice) are

$$\frac{\partial}{\partial t}\left[\sum_{p=l,g,i}\phi\omega_p^\beta n_p s_p\right] = -\sum_{p=l,g}\nabla\cdot\left[\omega_p^\beta n_p \mathbf{V}_p\right] + \sum_{p=l,g}\nabla\cdot\left[\phi\tau_p n_p D_p \nabla\omega_p^\beta\right] + S^\beta \quad (1)$$

where the Darcy velocity $\mathbf{V}_p$ is

$$\mathbf{V}_p = -\frac{k_{rp}k}{\mu_p}\left(\nabla P_p + \rho_p g \nabla z\right) \quad (2)$$

Here s is the phase saturation ($s_l + s_g + s_i = 1$), t is time, φ is porosity, n is density on a molar basis, ρ is mass density, ω is mole fraction, k is the absolute permeability, k_r is relative permeability, μ is dynamic viscosity, P is phase pressure, z is the vertical coordinate, g is the acceleration due to gravity, D is the diffusion coefficient, S is the mass source rate, and τ is the phase-dependent tortuosity. In this notation, "liquid phase" air should be interpreted as dissolved air. Ice-phase air is not tracked, so $\omega_i^a \equiv 0$. Note that the mole fractions satisfy the relation $\omega_p^a + \omega_p^w = 1$ for $p = l, g, i$.

The corresponding energy balance equation assumes local thermal equilibrium among the ice, liquid, gas and rock, leading to

$$\frac{\partial}{\partial t}\left[\sum_{p=l,g,i}\left(\phi\rho_p s_p u_p\right) + (1-\phi)\rho_{rock}u_{rock}\right] = -\sum_{p=l,g}\nabla\cdot(\rho_p h_p \mathbf{V}_p) + \nabla\cdot[\kappa_e \nabla T] + S_E \quad (3)$$

where T is temperature, u is specific internal energy, h is specific enthalpy, κ_e is the equivalent thermal conductivity for the rock–water–ice mixture, S_E is the thermal energy source, and the subscript *rock* denotes the solid (rock) phase.

Various constitutive relationships are needed to incorporate the non-isothermal phase dynamics of water and air. In particular, relationships are needed to describe equilibrium constraints for species dissolution in the liquid phase, to relate phase saturation with capillary pressure and permeability (for obtaining hydraulic conductivity), to estimate phase-dependent thermal conductivities of partially saturated media, as well as to estimate phase-dependent diffusive transport properties.

The empirical retention model by van Genuchten (1980) is used to relate capillary pressure P_c with liquid retention S_*,

$$S_*(P_c) = \left[1 + \left(\frac{P_c}{P_0}\right)^\nu\right]^{-\lambda} \quad \text{for } P_c > 0$$
$$S_*(P_c) = 1 \quad \text{for } P_c \leqslant 0 \quad (4)$$

where P_0 and $\lambda = 1-1/\nu$ are empirical curve fitting parameters. The retention model is combined with pair-wise relationships for saturation and interfacial-dependent capillary pressure, depending on interface (ice–liquid or liquid–gas), in order to obtain relationships between capillary pressure and liquid phase saturation s_l (Fig. 2a). That is, the retention curve for the liquid–ice system is

$$\frac{s_l}{s_l + s_i} = S_*\left(\frac{\sigma_{gl}}{\sigma_{il}}P_{cil}\right) \quad (5)$$

and the retention curve for the gas–liquid system is

$$\frac{s_l}{s_l + s_g} = S_*(P_{cgl}) \quad (6)$$

where σ_{gl} and σ_{il} are gas–liquid and ice–liquid interfacial tensions, P_{cgl} and P_{cil} are the gas–liquid and ice–liquid capillary pressures, respectively. In order to relate the ice–liquid capillary pressure to temperature and chemical composition of the liquid phase, the following approximation of Loch's model (Loch, 1977) is used

$$P_{cil} = -P_\Omega - \rho_i h_{iw}^0 \ln\left(\frac{T}{T_0}\right) \approx -P_\Omega - \rho_i h_{iw}^0 \frac{T - T_0}{T_0} \quad (7)$$

where h_{iw}^0 is the heat of fusion of water at $T_0 = 0$ °C, and P_Ω is the osmotic pressure. First, temperature T is used in (7) to obtain the ice-liquid capillary pressure P_{cil}; thereafter the retention relationship for S_* in (4) is combined with (5) to obtain liquid saturation index

s_l, (noting that $s_g + s_l + s_i = 1$); and finally this allows for the gas–liquid capillary pressure P_{cgl} to be obtained by inverting (6).

Mualem's model for relative permeability (Mualem, 1976) is combined with the van Genuchten retention model to relate liquid phase relative permeability k_{rl} with liquid phase saturation (Fig. 2b),

$$k_{rl} = (s_l)^{1/2}\left[1 - \left(1 - (s_l)^{1/\lambda}\right)^{\lambda}\right]^2 \tag{8}$$

Since the gas phase has a much lower viscosity than water, gas is relatively free to move and results are generally not sensitive to choice of model for gas-phase permeability; a simple linear assumption $k_{rg} = s_g$ is used to relate gas relative permeability with gas phase saturation.

It is important to note that the unfrozen water content and the relative permeability to liquid water at all temperatures are fully specified by the chosen capillary pressure and relative permeability relationships for *unfrozen* conditions. That is, hydraulic conductivity is obtained from the liquid saturation index, which in turn decreases with temperature below the nominal freezing temperature, since the liquid-available pore space decreases with increasing ice phase saturation index. This formulation, which relies on thermodynamic constraints and well-established models for dynamics of three fluid phases in porous media, is in contrast to previous models of freezing in soils that rely on purely empirical fits to the unfrozen water fraction and empirical "blocking factor" adjustments to the relative permeability curves below the nominal freezing temperature. That empirical freezing characteristic curves are not required is important because these are not as widely available as the familiar characteristic curves for unfrozen media, which have been compiled for many soil types.

The equivalent thermal conductivity κ_e of the rock–water–ice media is obtained from both the liquid and ice phase saturation levels as

$$\kappa_e = \mathrm{Ke}_f \kappa_{sat,f} + \mathrm{Ke}_u \kappa_{sat,u} + (1 - \mathrm{Ke}_f - \mathrm{Ke}_u)\kappa_{dry} \tag{9}$$

where $\kappa_{sat,f}$ and $\kappa_{sat,u}$ are the thermal conductivities for frozen and unfrozen media under saturated conditions, κ_{dry} is the dry (unsaturated) conductivity, and Ke_f and Ke_u are the Kersten numbers for frozen and unfrozen conditions, respectively. The Ke_f and Ke_u parameters depend on ice and liquid content, respectively; power-law fits in s_i and s_l capture the general trends and provide sufficient flexibility (Painter, 2011). However, it is acknowledged that dependence of thermal conductivity on ice and liquid content may vary from site to site. Also, $\kappa_{sat,f}$ and $\kappa_{sat,u}$ are related to porosity and thermal conductivities for ice and liquid phase water using the proposed empirical fits by Andersland and Ladanyi (1994). The dry conductivity is related to porosity and thermal conductivities for mineral grains using relationships proposed by Peters-Lidard et al., (1998).

The resulting conservation equations are solved by adopting an integral finite difference method with fully implicit time stepping. Further details on the numerical approach and application of constitutive relations are described by Painter (2011).

2.2. Permafrost simulation scenarios

The simulation domain configuration considered in this study represents a two-dimensional soil section (Fig. 1) with a depth below the land surface of either 20 m or 30 m, depending on simulation case. The top boundary is open to flow (surface infiltration) and has an assigned annual variation in temperature. The bottom boundary is closed to flow and has a specified geothermal flux boundary condition. The left boundary is no-flow by symmetry. A seepage face condition is imposed at the right boundary by specifying gas pressure and temperature, and setting capillary pressure to zero. In order to represent an unfrozen region near a river (a river talik), the seepage face boundary condition is treated as follows. The temperature at the base of the seepage face is set to 0.5 °C, at the top it is set to the imposed annual variation in temperature, and then linear interpolation is used between the top and bottom to assign temperature along its depth.

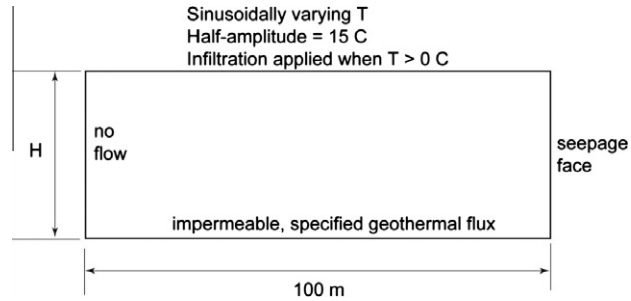

Fig. 1. The simulation domain and boundary conditions.

Table 1
Physical properties assigned to the three soil types used and combined in the simulations.

Soil type	Porosity (–)	Liquid saturated thermal conductivity (W/m K)	Mineral phase specific heat capacity (J/kg K)	Saturated hydraulic conductivity K (m/s)
Silt	0.45	1.3	837	7.1×10^{-7}
Silty sand	0.38	1.5	750	3.2×10^{-6}
Sand	0.25	1.68	620	2.5×10^{-5}

Table 1 shows the different soil properties, across a range typical for silt, silty sand and sand, which were used and combined in the simulations to represent different types of homogeneous and heterogeneous soil formations. Fig. 2 shows the constitutive relationships used for capillary pressure and hydraulic conductivity

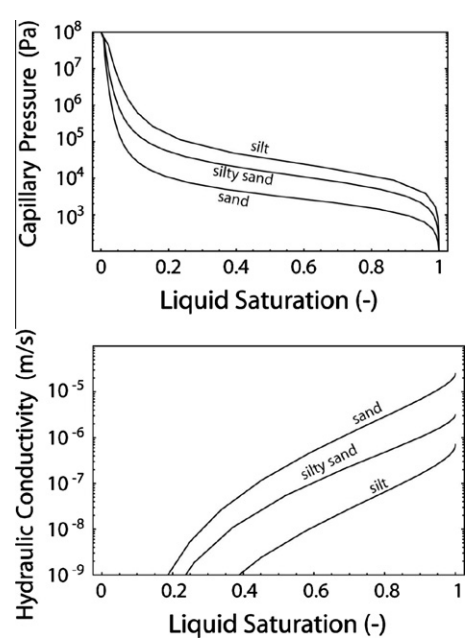

Fig. 2. The applied relationships between water saturation and capillary pressure (upper) as well as water saturation and hydraulic conductivity (lower) for the three soil types used in simulations.

Table 2
The simulation scenarios considered.

Case	Soil type	Infiltration rate I (mm/year)	Domain depth (m)	I/K (–)
Sand1	Sand	750	20	0.001
Silt1	Silt	50	20	0.002
Silt5	Silt	50	30	0.002
SiltySand1	Silty sand	700	20	0.007
SiltySand5	Silty sand	700	30	0.007
SiltySand5a	Silty sand	100	30	0.001
Discon5	Silty sand on right half and Sand on left half	100	30	0.0002
TwoLayer5	5 m layer of silty sand on top of silt	100	30	0.001

to water saturation for the soil textures considered. Table 1 also lists hydraulic and thermal properties assigned to the different soil textures, and Table 2 outlines the simulation scenarios considered, where different combinations of soil types, surface infiltration rates and domain depths are investigated. These were chosen in order to investigate a selection of representative subsurface configurations found in many arctic and subarctic environments on Earth. This is a first-order approximation and, of course, other possible configurations could also be encountered in these environments.

In each case considered, the permafrost formation and degradation under variable and changing surface temperature is simulated, and the resulting water fluxes within and out from the soil domain through a seepage face boundary is calculated. The water flux through the seepage face represents groundwater discharge into a surface water body such as a river. Each simulation has two phases. In the first phase, the temperature at the soil surface varies sinusoidally with a 1-year period, an annual mean of −1 °C, and a peak-to-trough amplitude of 30 °C. Water is introduced into the model as infiltration through the top boundary and depends on the assigned annual infiltration rate (Table 2). Also, infiltration is applied as liquid water during non-freezing surface temperatures only, keeping the net infiltration rate constant. Effects of accumulated snowfall and snowmelt are not included in these initial simulations. This means seasonal events such as snowmelt and intense rainfall are averaged out and equally distributed over the non-freezing periods. The first-phase simulations start from an arbitrary initial state and stop when a periodic steady state is reached for water flow, which typically requires simulation periods of hundreds of years. This periodic steady state allows for a stable scenario where generally a seasonally changing active layer develops to a certain depth, and a clear permafrost region being constantly maintained beneath it.

The results from the first phase are used as initial conditions in the second phase, simulating 100 years with a warming trend of 0.01 °C per year. This allows for the simulation of soil water and groundwater flow responses to a long-term increase (in addition to the seasonal variability) of surface temperature, as could be expected, for example, under future climatic changes. Again, this is a generic trend considered as a potential future scenario. The magnitude of such an increasing trend is reasonable, based on previous work (e.g., Lyon et al., 2009), with specific testing of different trends and amplitudes of temperature fluctuations being outside the scope of this first study.

3. Results

Fig. 3 shows snapshots of permafrost and water conditions at the periodic steady state phase (i.e. without a warming trend) for three soil formation examples. As seen for instance for the case of homogeneous silty sand (SiltySand5), permafrost has formed at depths of approximately 3–5 m. The active layer exists above that depth range, a frozen vadoze zone lies below the ice-saturated layer, and the groundwater table and a thin aquifer lie below the vadoze zone. During the summer months, a thin aquifer is also perched on the ice layer and water is diverted toward the seepage face. However, along most of the seepage face, water saturation is not reached which results in no or little discharge. Instead, flow in the unfrozen region near the seepage face is primarily vertical and recharges the underlying aquifer, with only water from that aquifer discharging through the seepage face.

In the case of homogeneous sand (Sand1, Fig. 3), the relatively high saturated hydraulic conductivity, K, and low capillary pressure of the sand allow water to drain rapidly when infiltration stops in the winter months. For these conditions, no ice-saturated layer forms. In a heterogeneous formation case with sand on the left half and silty sand on the right half of the simulation domain (Discon5, Fig. 3), a permanent ice-saturated layer does form, but only in part of the domain, yielding discontinuous permafrost. In this case, infiltrating water that is blocked by the permanent ice layer in the silty sand region flows both to the left and below the frozen layer, as well as to the right and above it, yielding a bimodal distribution of flow paths to the seepage face.

Fig. 4 shows the long-term development of seepage flux with time after start of the warming trend. Results are exemplified for the three textures SiltySand, Discon and TwoLayer in the domain size with depth 30 m. For the SiltySand texture, a comparison is made for two values of the fraction I/K, where I is the net infiltration rate at the surface, and K is the saturated hydraulic conductivity in the subsurface formation (cf Table 2). The top panels in Fig. 4 show the evolution of annual flow variability over ten decades after the warming trend is initiated. The middle panels show the development of annual maximum and minimum fluxes for the entire warming trend (i.e. during the 100 years), and the lower panels show seasonal and annual average seepage fluxes for the warming trend period.

By comparing SiltySand5 ($I/K = 0.007$) with SiltySand5a ($I/K = 0.001$), we see that a smaller I/K fraction yields smaller differences between annual maximum and minimum flux (Fig. 4, middle panels), and generally leads to smaller temporal flow variability (top panels) as well as smaller differences between seasonal average fluxes (bottom panels). This is also evident by considering Discon5, which has an even lower $I/K = 0.0002$, albeit representing a different soil texture.

Next consider the cases SiltySand5a (homogeneous silty sand texture) and TwoLayer5 (heterogeneous formation with a 5 m layer of silty sand on top of silt), which have the same I/K fraction. The layering in the latter case yields preferential flow through the thin, relatively high-conductive, upper silty sand layer. This preferential flow formation yields greater flow variability, seen as greater differences between the seasonal average fluxes (bottom panels), than in the comparative case of a homogeneous silty sand.

Comparisons between the homogeneous formation cases SiltySand and Silt with different domain depths are provided in Figs. 5 and 6 respectively. These results show that a smaller depth extent

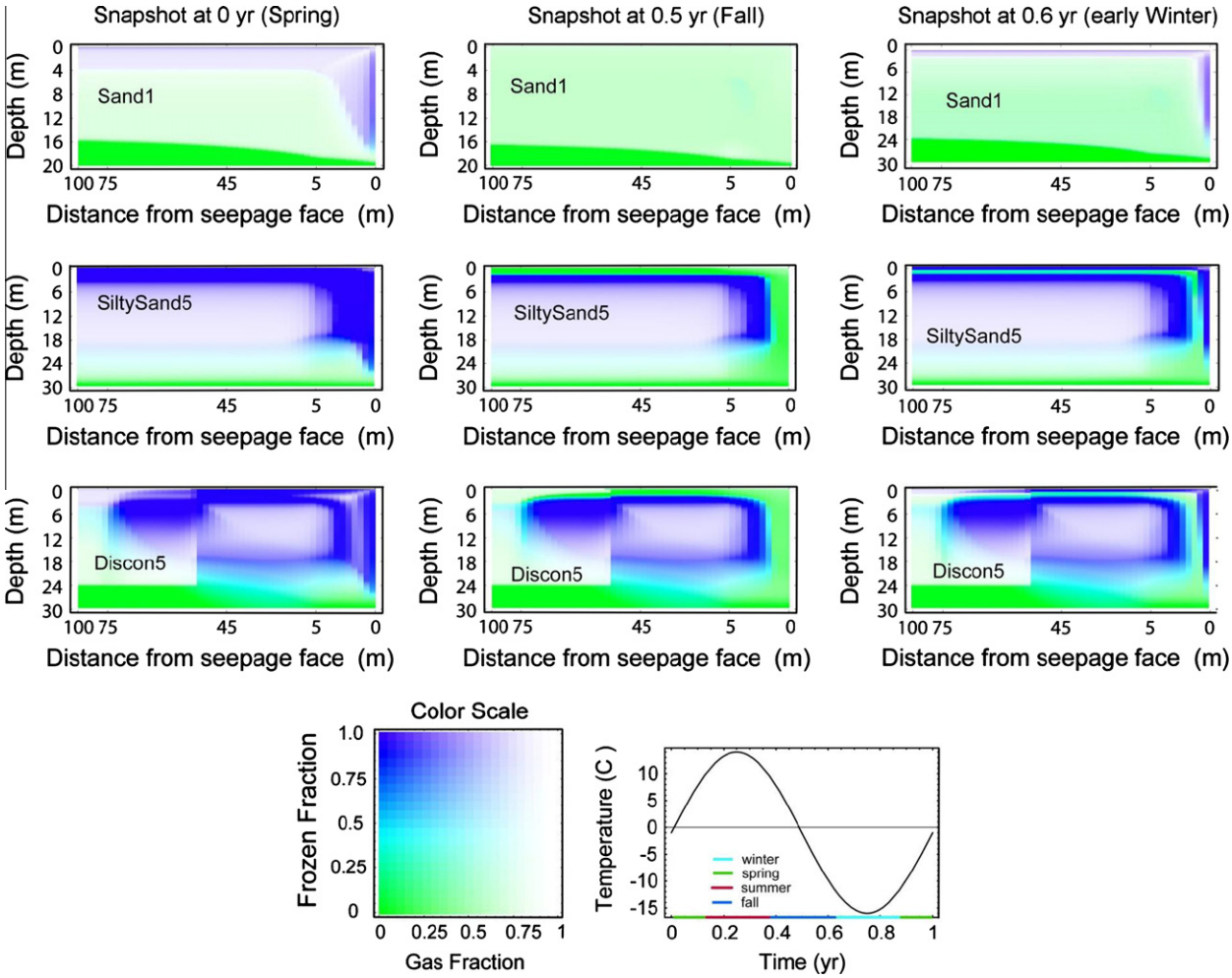

Fig. 3. Snapshots showing frozen and gas fractions in the domain during the periodic steady state phase for three simulation cases. The simulation scenarios are explained in the main text and Table 2. Note the distorted horizontal scale, which emphasises and allows details to be seen near the seepage face on the right.

of the flow domain (20 m, right columns) yields greater temporal flow variability than the greater depth (30 m, left columns), a result that is consistent with findings from subsurface flow studies in non-permafrost regions (Prieto et al., 2006).

Simulation cases with large I/K ratios (cases SiltySand1 and SiltySand5 in Fig. 5) and/or small formation depths (cases SiltySand1 and Silt1 in Figs. 5 and 6 respectively) also exhibit occasional transient spikes in their pre-warming flow variability over the year, which disappear with the warming trend (cf upper panels). Such spikes are due to saturated conditions occasionally being reached and yielding groundwater discharge relatively high up on the seepage face, whereas the rest of the time groundwater discharge is purely from the lower aquifer. Besides these occasional transient spikes, the seepage fluxes generally peak in Fall (~0.5 year) and are smallest in Spring (~0 year and 1 year), as can be seen from the top rows of Figs. 4–6. In the pre-warming periodic steady-state phase, the main seepage flux peak typically lags the surface temperature peak by about 0.25 years. The warming trend generally increases this lag, as is clearly visible e.g. for the case TwoLayer5 in Fig. 4, further delaying the main flow peak in the fall relative to the main temperature peak in the summer.

4. Discussion and conclusions

Based on the model results obtained in this study, permafrost spreading and continuity may notably depend on subsurface hydraulic properties, in addition to the temperature conditions that are often used as an only base for characterizing permafrost conditions in absence of comprehensive direct permafrost measurements over large scales. Specifically, for the same present surface temperature conditions, a locally continuous permafrost region forms in low-conductive soils, while no permafrost forms in high-conductive soils, and locally discontinuous permafrost forms in heterogeneous soils.

Independently of subsurface properties, however, permafrost degradation due to a warming trend consistently decreases the seasonal variability of groundwater discharge into surface waters. The tendency toward episodic flows is also reduced. This decreased seasonal variability is the result of increased active layer depth, which allows more water to flow in between discontinuous permafrost parts down to the deeper aquifer before discharging into surface water. As a consequence, the warming trend and permafrost thawing increase the depth and length of subsurface flow paths, and the lag-times of subsurface water flow from infiltration or permafrost thawing to surface water discharge. These main results and implications are schematically illustrated in Fig. 7.

Permafrost change is difficult to observe directly on large scales. Even where direct permafrost observations are made today, they need to be compared with typically unavailable corresponding observations from the past in order to determine changes in the permafrost. This study has demonstrated the usefulness and importance of applying three-phase, temperature dependent flow

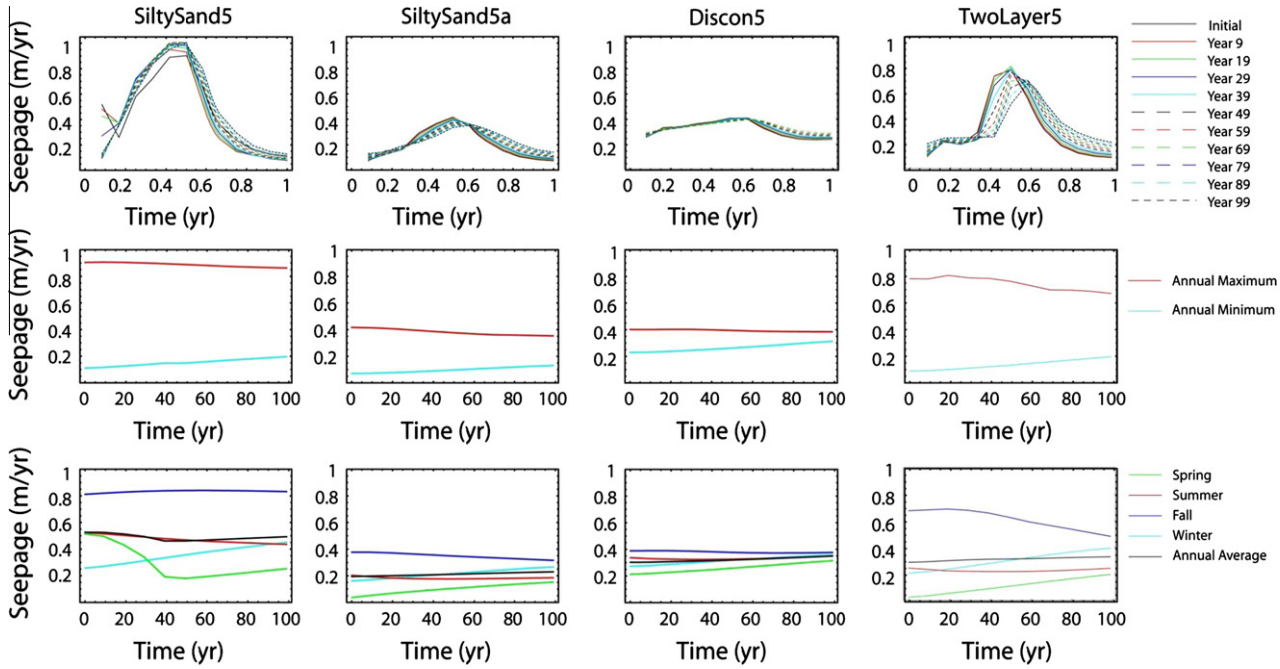

Fig. 4. Long-term development of seepage flux with time after start of the warming trend for five simulation case examples with various soil textures and I/K fractions. *Upper panels*: the evolution of annual flow variability over ten decades after the warming trend is initiated. *Middle panels*: annual maximum (red) and minimum (cyan) flows for the duration of the ten decades. *Lower panels*: seasonal average flows (blue: autumn; cyan: winter; green: spring; red: summer; black: mean annual) over the ten decades. The illustrated cases are homogeneous silty sand formations with $I/K = 0.007$ (SiltySand5) and $I/K = 0.001$ (SiltySand5a); a heterogeneous formation with silty sand the right half (closest to the seepage face) and sand on the left half with average $I/K = 0.0002$ (Discon5); and a dual layered formation consisting of silty sand with $I/K = 0.001$ on top of silt (TwoLayer5). A summary of the simulation configuration details is given in Table 2.

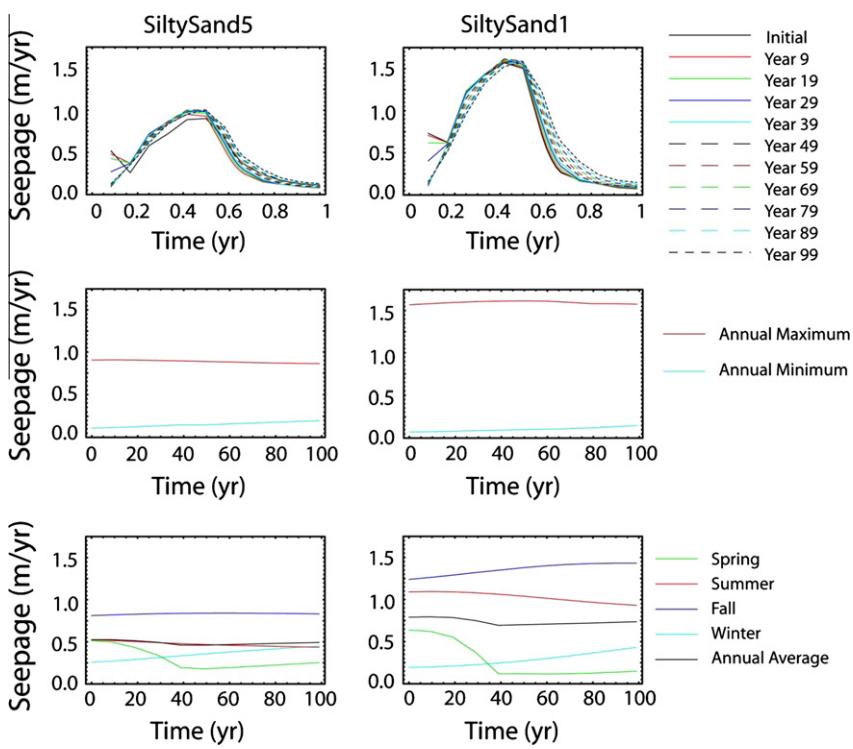

Fig. 5. Long-term development of seepage flux with time after start of the warming trend for a homogeneous silty sand formation. Comparing the effect of domain depths 30 m (SiltySand5) and 20 m (SiltySand1), both with $I/K = 0.007$ (cf Table 2). *Upper panels*: the evolution of annual flow variability over ten decades after the warming trend is initiated. *Middle panels*: annual maximum (red) and minimum (cyan) flows for the duration of the ten decades. *Lower panels*: seasonal average flows (blue: autumn; cyan: winter; green: spring; red: summer; black: mean annual) over the ten decades.

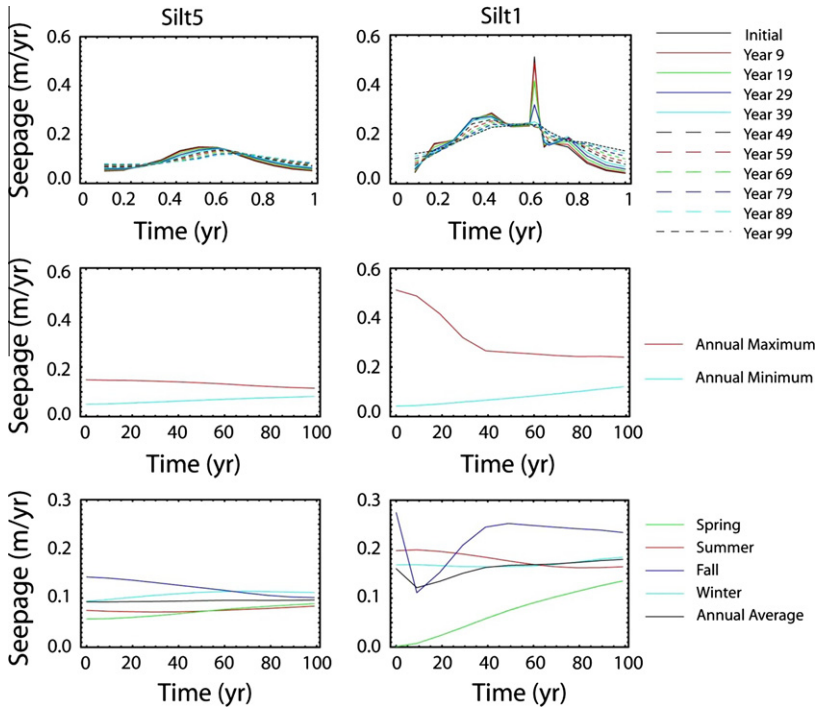

Fig. 6. Long-term development of seepage flux with time after start of the warming trend for a homogeneous silt formation. Comparing the effect of domain depths 30 m (Silt5) and 20 m (Silt1), both with $I/K = 0.002$ (cf Table 2). *Upper panels*: the evolution of annual flow variability over ten decades after the warming trend is initiated. *Middle panels*: annual maximum (red) and minimum (cyan) flows for the duration of the ten decades. *Lower panels*: seasonal average flows (blue: autumn; cyan: winter; green: spring; red: summer; black: mean annual) over the ten decades.

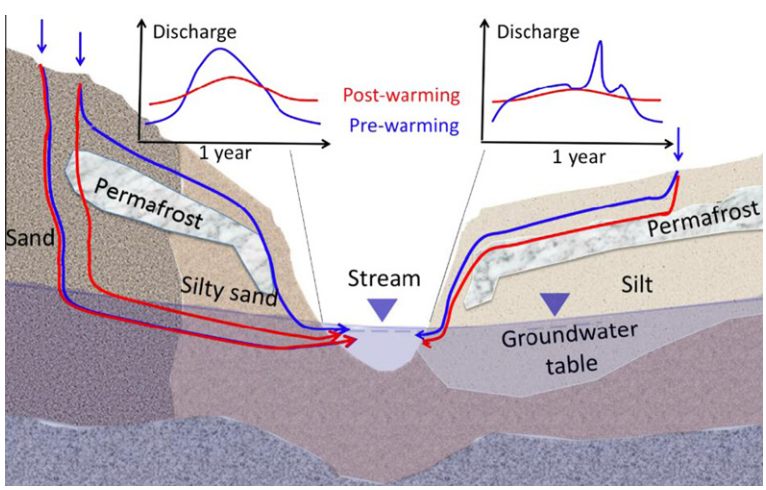

Fig. 7. Schematic illustration of main simulation results and their implications. The subsurface hydraulic properties and heterogeneity control the formation and continuity of permafrost, as well as its seasonal variability and episodic effects on subsurface runoff to surface waters. For all subsurface conditions, the common main hydrological flow signal of permafrost degradation in a warming trend (from blue to red flow paths/discharge) is decreasing seasonal flow variability, due to deeper and longer subsurface flow paths and increasing lag times of subsurface water flow from infiltration or permafrost thawing to surface water discharge.

modelling, as this allows for systematic investigations to be conducted on the responses of permafrost hydrology to climate variability and climate change, under different local and regional soil conditions. Furthermore, it has shown how permafrost change may be reflected in, and thereby detected through its effects on hydrological flows.

Long-term hydrological observation records are often available and can be used to detect different types of permafrost change reflections and indicators in these records. Previous studies have identified changes in temporal variability of the base flow from groundwater as one indicator of permafrost change (Brutsaert, 2008; Lyon et al., 2009; Lyon and Destouni, 2010). The present results of consistent decrease in temporal flow variability during permafrost thawing across a range of different conditions point at another possible such indicator. Moreover, the results of groundwater flow paths becoming deeper and longer during permafrost thawing point at additional indicator possibilities, for instance, increasing dissolved inorganic carbon concentrations in stream

water due to increasing weathering products along longer flow paths (Walvoord and Striegl, 2007; Lyon et al., 2010). A range of such different indicators can thus be identified and further investigated by physically based modelling of permafrost hydrology for increasingly more complex/realistic model system conditions, and by direct comparison of such model results and implications with available hydrological data, to increase the understanding and check the reliability of various permafrost change interpretations.

As is the case with all modelling, also the present model analysis is simplified and limited. The modelled scenarios consider only a relatively moderate imposed temperate regime (sinusoidally varying annual mean temperature of −1 °C and half-amplitude of 15 °C, to represent an example seasonal variability in surface temperature), a relatively mild climate change scenario (with annual mean temperature gradually increasing from −1 °C to 0 °C over a 100 year period, to represent an example long-term change development in surface temperature), and constant water infiltration rates at the soil surface (to represent various examples of mean annual infiltration conditions, but with no other variability than that related to temperature considered in these hydrological conditions, in order to here clearly distinguish the specific temperature variability and change effects on flow variability). Relaxing, for example, the latter condition in new simulation scenarios, by considering also seasonal variation and small-scale temporal fluctuations in the surface infiltration rate, may for some site conditions yield results where the presently found consistent decrease in temporal flow variability during permafrost thawing is overwhelmed and hidden by the added infiltration variability. The modelling approach of this study can then be further used to systematically relax different simplifying assumptions, and identify under which conditions such relaxation leads to different implications for the detection and interpretation of permafrost change through hydrological records. Even with its limitations, the present study illustrates the strength and capabilities of adopting physically-based numerical models to improve understanding of the interactions between permafrost change and changes in near-surface water flow dynamics, and highlights the scientific and practical need to use available field data for directly checking such model-implied change interactions under the changing climate in arctic and subarctic regions.

Acknowledgements

This study was funded by the Swedish Research Council (VR) and the Swedish Geological Survey. The work was carried out within the framework of the Bert Bolin Centre for Climate Research, which is supported by a Linnaeus grant from VR and The Swedish Research Council Formas. Cynthia Dinwiddle at the Southwest Research Institute provided assistance with the definition of typical soil properties.

References

Andersland, O.B., Ladanyi, B., 1994. An Introduction to Frozen Ground Engineering. Chapman and Hall, New York.
Anisimov, O., Reneva, S., 2006. Permafrost and changing climate: the Russian perspective. Ambio 35, 169–175.
Arctic-HYDRA (2010). The Arctic Hydrological Cycle Monitoring, Modelling and Assessment Programme, Science and Implementation, Grafia Kommunikasjon AS, Oslo. ISBN 978-9979-9975-0-4.
Bense, V.F., Ferguson, G., Kooi, H., 2009. Evolution of shallow groundwater flow systems in areas of degrading permafrost. Geophysical Research Letters 36, L22401. doi:10.1029/2009GL039225.
Bring, A., Destouni, G., 2009. Hydrological and hydrochemical observation status in the Pan-Arctic drainage basin. Polar Research 28, 327–338.
Brutsaert, W., 2008. Long-term groundwater storage trends estimated from streamflow records: climatic perspective. Water Resources Research 44, W02409.
Carey, S.K., Woo, M.K., 2001. Slope runoff processes and flow generation in a subarctic, subalpine catchment. Journal of Hydrology 253, 110–129.
Cui, X., Graf, H., 2009. Recent land cover changes on the Tibetan Plateau: a review. Climatic Change 94, 47–61.
Dyurgerov, M., Bring, A., Destouni, G., 2010. Integrated assessment of changes in freshwater inflow to the Arctic Ocean. Journal of Geophysical Research 115, D12116. doi:10.1029/2009JD013060.
Francis, J.A. et al., 2009. An arctic hydrologic system in transition: feedbacks and impacts on terrestrial, marine, and humanlife. Journal of Geophysical Research 114, G04019.
Frey, K.E., McClelland, J.W., 2009. Impacts of permafrost degradation on arctic river biogeochemistry. Hydrological Processes 23, 169–182.
Grimm, R.E., Painter, S.L., 2009. On the secular evolution of groundwater on Mars. Geophysical Research Letters 36, L24803.
Hinzman, L.D. et al., 2005. Evidence and implications of recent climate change in Northern Alaska and Other Arctic Regions. Climatic Change 72, 251–298.
Loch, J.P.G., 1977. Thermodynamic equilibrium between ice and water in porous media. Soil Science 126, 77–80.
Lyon, S., Destouni, G., 2010. Changes in catchment-scale recession flow properties in response to permafrost thawing in the Yukon River Basin. International Journal of Climatology 30(14), 2138–2145, doi:10.1002/joc.1993.
Lyon, S.W. et al., 2009. Estimation of permafrost thawing rates in a sub-arctic catchment using recession flow analysis. Hydrology and Earth Systems Sciences 13, 595–604.
Lyon, S.W., Mörth, M., Humborg, C., Giesler, R., Destouni, G., 2010. The relationship between subsurface hydrology and dissolved carbon fluxes for a sub-arctic catchment. Hydrology and Earth System Sciences 14, 941–950.
MacLean, R.M., Oswood, M.W., Irons III, J.G., McDowell, W.H., 1999. The effect of permafrost on stream biogeochemistry: a case study of two streams in the Alaskan (USA) taiga. Biogeochemistry 47, 239–267.
Manabe, S., Milly, P.C.D., Wetherald, R., 2004. Simulated long-term changes in river discharge and soil moisture due to global warming. Hydrological Sciences Journal 49, 625–642.
McClelland, J.W., Déry, S.J., Peterson, B.J., Holmes, R.M., Wood, E.F., 2006. A pan-arctic evaluation of changes in river discharge during the latter half of the 20th century. Geophysical Research Letters 33, L06715.
McNamara, J.P., Kane, D.L., Hobbie, J., Kling, G.W., 2008. Hydrologic and biogeochemical controls on the spatial and temporal patterns of nitrogen and phosphorus in an Arctic river. Hydrological Processes 17, 3294–3309.
Mualem, Y., 1976. A new model for predicting the hydraulic conductivity of unsaturated porous media. Water Resources Research 12, 513–522.
Nelson, F.E., 2003. Geocryology: enhanced: (un)frozen in time. Science 299, 1673–1675.
Painter, S.L., 2011. Three-phase numerical model of water migration in partially frozen geological media: model formulation, validation, and applications. Computational Geosciences 15, 69–85. doi:10.1007/s10596-010-9197-z.
Painter, S.L., Grimm, R.E., 2007. Three-phase simulations of moisture movement in the Martian subsurface. In: Albee, A.L., Kieffer, H.H. (Eds.), Sixth International Conference on Mars, July 20–25, 2003, Pasadena, California, p. 3272 (Lunar and Planet. Inst., Houston, Texas).
Peters-Lidard, C.D., Blackburn, E., Liang, X., Wood, E.F., 1998. The effect of thermal conductivity parameterization on surface energy fluxes and temperatures. Journal of Atmospheric Science 55, 1209–1224.
Peterson, B.J. et al., 2002. Increasing river discharge to the Arctic Ocean. Science 298, 2171–2173.
Prieto, C., Kotronarou, A., Destouni, G., 2006. The influence of temporal hydrological randomness on seawater intrusion in coastal aquifers. Journal of Hydrology 330, 285–300.
Riseborough, D., Shiklomanov, N., Etzelmüller, B., Gruber, S., Marchenko, S., 2008. Recent advances in permafrost modelling. Permafrost and Periglacial Processes, 19, 137–156, doi:10.1002/ppp.615
Smedberg, E., Morth, C.-M., Swaney, D.P., Humborg, C., 2006. Modelling hydrology and silicon-carbon interactions in taiga and tundra biomes from a landscape perspective: implications for global warming feedbacks. Global Biogeochemical Cycles 20, GB2014.
van Genuchten, M.Th., 1980. A closed-form equation for predicting the hydraulic conductivity of unsaturated soils. Soil Science Society of America Journal 44, 892–898.
Woo, M., Kane, D.L., Carey, S.K., Yang, D., 2008. Progress in permafrost hydrology in the new millennium. Permafrost and Periglacial Processes 19, 237–254.
Wu, P.L., Wood, R., Stott, P., 2005. Human influence on increasing Arctic river discharges. Geophysical Research Letters L02703 (2005).
Yamazaki, Y., Kubota, J., Ohata, T., Vuglinsky, V., Mizuyama, T., 2006. Seasonal changes in runoff characteristics on a permafrost watershed in the southern mountainous region of eastern Siberia. Hydrological Processes 20, 453–467.
Walvoord, M.A., Striegl, R.G., 2007. Increased groundwater to stream discharge from permafrost thawing in the Yukon River basin: potential impacts on lateral export of carbon and nitrogen. Geophysical Research Letters 34, L12402.
Zhang, T. et al., 2005. Spatial and temporal variability in active layer thickness over the Russian Arctic drainage basin. Journal of Geophysical Research 110, D16101.